

MoS₂/Celgard Separator as Efficient Polysulfide Barrier for Long-Life Lithium–Sulfur Batteries

Zahid Ali Ghazi, Xiao He, Abdul Muqsit Khattak, Niaz Ali Khan, Bin Liang, Azhar Iqbal, Jinxin Wang, Haksong Sin, Lianshan Li,* and Zhiyong Tang*

A high lithium conductive MoS₂/Celgard composite separator is reported as efficient polysulfides barrier in Li–S batteries. Significantly, thanks to the high density of lithium ions on MoS₂ surface, this composite separator shows high lithium conductivity, fast lithium diffusion, and facile lithium transference. When used in Li–S batteries, the separator is proven to be highly efficient for depressing polysulfides shuttle, leading to high and long cycle stability. With 65% of sulfur loading, the device with MoS₂/Celgard separator delivers an initial capacity of 808 mAh g⁻¹ and a substantial capacity of 401 mAh g⁻¹ after 600 cycles, corresponding to only 0.083% of capacity decay per cycle that is comparable to the best reported result so far. In addition, the Coulombic efficiency remains more than 99.5% during all 600 cycles, disclosing an efficient ionic sieve preventing polysulfides migration to the anode while having negligible influence on Li⁺ ions transfer across the separator. The strategy demonstrated in this work will open the door toward developing efficient separators with flexible 2D materials beyond graphene for energy-storage devices.

With the rapid development of portable electronic devices and electric vehicles, the demand for research on advanced energy-storage systems with low cost and high energy density has significantly increased to replace the traditional lithium-ion batteries (LIBs), which are limited by their low energy density.^[1,2] Accordingly, lithium–sulfur (Li–S) batteries have attracted great interest due to their exceptional theoretical capacity (1672 mAh g⁻¹) and specific energy density (2600 Wh kg⁻¹) compared to state-of-the-art LIBs.^[3] Despite their great potential, Li–S battery systems suffer from several drawbacks that severely impede the practical application. The major one is the so-called “shuttle effect” caused by dissolution of the discharge/charge intermediates, e.g., the high-order lithium polysulfides (LiPSs)

(Li₂S_{*n*}, 4 ≤ *n* ≤ 8) in organic electrolytes and their free migration between the cathode and anode. These dissolved high-order PSs move toward the anode and react with the lithium metal to produce low-order PSs; subsequently, as-generated low-order PSs move back to the cathode and form high-order PSs again, consequently resulting in capacity loss of the sulfur cathode and poor cycle life of the battery.^[4,5] In addition, the shuttle process also passivates lithium anode, giving rise to limited rate performance and sulfur utilization.

Different strategies have been employed to reduce the shuttle effect and improve the retention of active materials within the sulfur electrode. One of the most effective strategies is to constrain sulfur or LiPSs within cavities to keep the mechanical and electrical integrity of the elec-

trodes, and many nanostructures have been examined as host materials including various microporous carbons,^[6,7] carbon nanotubes,^[8,9] carbon nanofibers,^[5,10] carbon spheres,^[11] graphene,^[12] and conductive polymers.^[13–16] Furthermore, new crystalline porous materials, e.g., metal-organic frameworks (MOFs) and covalent organic frameworks (COFs) with low density, small pore size, and large surface area, are also used as host material for sulfur storage.^[17–19] Cathodes based on these nanoarchitectures have proven to significantly depress shuttle effect, enhance the sulfur utilization, and improve the cycle stability and rate capabilities. However, the cycle stability obtained to date has still been far from satisfactory from commercial view point, and the Coulombic efficiencies fall down to 75%–85% after 200–300 cycles in most cases. Moreover, the structural change due to volume expansion on discharge can further degrade the sulfur cathode.^[20,21] Most importantly, depressing PSs shuttle by porous host is at the cost of losing energy density since porous host could not contribute any capacity. Usually, as high as 30–60 wt% of host materials are needed to efficiently depress PSs shuttle in sulfur/porous host composite cathode, which means about 20%–50% of energy loss compared to pure sulfur/carbon black cathode with 70% of S loading. Obviously, though the use of porous materials would suppress the PSs shuttle, the low sulfur loading greatly offsets the advantage of high energy density of Li–S battery. Therefore, research on development of novel materials and advanced strategies, which can not only block PSs shuttle but also increase the sulfur loading in the cathode, is highly desirable. This

Z. A. Ghazi, X. He, A. M. Khattak, Dr. N. A. Khan, Dr. B. Liang, A. Iqbal, J. Wang, H. Sin, Prof. L. Li, Prof. Z. Y. Tang
CAS Key Laboratory of Nanosystem and Hierarchical Fabrication
CAS Center for Excellence in Nanoscience
National Centre for Nanoscience and Technology
Beijing 100190, P. R. China
E-mail: lils@nanoctr.cn; zytang@nanoctr.cn



Z. A. Ghazi, X. He, A. M. Khattak, Dr. N. A. Khan, Dr. B. Liang, A. Iqbal, J. Wang, H. Sin, Prof. L. Li, Prof. Z. Y. Tang
University of Chinese Academy of Sciences
19 A Yuquan Rd, Shijingshan District, Beijing 100049, P. R. China

DOI: 10.1002/adma.201606817

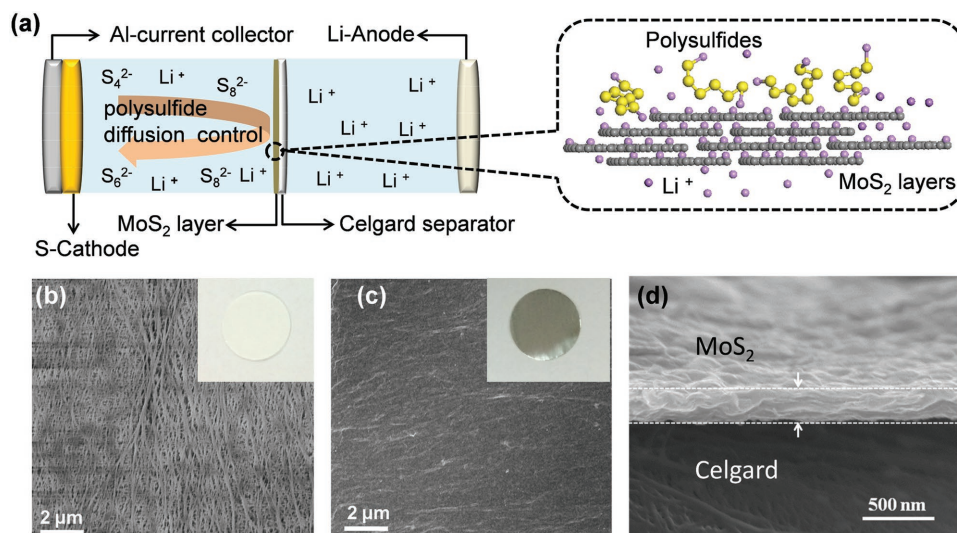


Figure 1. a) Schematic cell configuration of Li-S batteries using MoS₂/Celgard separator. b) SEM images of Celgard surface, c) MoS₂/Celgard surface (insets in panels (b) and (c) are photographs of pristine Celgard and MoS₂-coated Celgard, respectively), and d) cross section of MoS₂ layers.

requirement might be satisfied by introduction of a novel separator between two electrodes. In most cases, the separator is a porous membrane (e.g., polypropylene, polyethylene, glass fibers), which serves solely as an electronic insulator and does not influence the transportation of ions through the membranes. Unfortunately, PSs can diffuse freely through these separators and react with the anode, which can cause degradation of the battery. If a cation selective separator is introduced into the Li-S battery, the PSs anion would not diffuse through the separator, and the shuttle of PSs between the cathode and anode would be fully suppressed. Currently, the most widely used interlayers/separators include graphene, graphene-oxide coated separators,^[21,22] graphene interlayers,^[23] graphene foam, etc.^[24] In addition, calcined filter paper, carbon nanotube-COFs composite separators, ceramic, and metal oxide based separators have also been employed in this approach.^[25–28] However, these separators suffer either from poor lithium ions conductivity or low efficiency to block PSs due to their large pores. Impressively, a recent work demonstrated that when utilized as an ionic sieve, MOF@graphene oxide (MOF@GO) separator was able to selectively sieve lithium ions while efficiently suppress undesired PSs migration.^[29] However, although a Li-S battery with low capacity decay rate and long life cycle was successfully achieved using MOF@GO separator, 30% of CMK-3 porous host was still needed. In addition, fragility, poor lithium ion/electrical conductivity of MOFs and difficulty in formation of thin membranes still hinder their uses as ideal separator/interlayer in practical Li-S batteries.

Here, we report a simple strategy by using high lithium conductive MoS₂ membrane as new PSs barrier in Li-S batteries. The remarkable flexibility and unique optoelectronic property of MoS₂ engender a versatility of its application in many scientific fields such as thin film transistors,^[30] photovoltaic devices,^[31] supercapacitors, and lithium-ion batteries.^[32] Thanks to 2D flexible characteristics, MoS₂ thin layer is easily deposited on conventional Celgard separator by simple filtration to obtain a flexible MoS₂/Celgard composite separator (Figure S1, Supporting

Information). When used in Li-S batteries, this barrier could block the PSs diffusion, thereby significantly suppress the PSs shuttle and result in high Coulombic efficiency (Figure 1a). Meanwhile, due to excellent lithium ion conductivity the composite separator facilitates the transport of lithium ions, which guarantees the long life cycle and good rate capability of Li-S batteries.

High lithium conductive MoS₂ nanosheets were synthesized by lithium ion intercalation methods according to previous reports.^[33,34] Scanning electron microscope (SEM) and transmission electron microscope images show that after exfoliation the morphology of bulk MoS₂ changes to highly scattered nanosheets (Figure S2a–d, Supporting Information). X-ray photoelectron spectroscopy (XPS) analysis (Figure S2e, Supporting Information) reveals partial conversion of semi-conducting 2H phase to metallic 1T phase with a peak ratio of 2:3.^[33] The polarized surface of as-synthesized MoS₂ nanosheets makes them highly dispersible in aqueous solvents and affordable to be easily processed into ultrathin membranes with simple vacuum filtration techniques.^[34] Hence, lithium ion conductive MoS₂ membranes with different thickness were fabricated by vacuum filtering different amount of exfoliated MoS₂ suspension onto conventional Celgard separator. The corresponding SEM images of pure Celgard and MoS₂/Celgard composite separators are presented in Figure 1b and c. It is seen that pure Celgard surface possesses abundant of pores with diameters up to several hundred nanometers (Figure 1b). After coating with MoS₂, the pores are completely covered by nanosheets (Figure 1c). The cross section image further displays that the membrane is composed of closely stacked MoS₂ nanosheets with thickness of around 350 nm (Figure 1d). For comparison, the graphene oxide membrane with similar thickness was also fabricated (Figure S2f, Supporting Information).

The lithium ion conductivity of MoS₂/Celgard separator was first evaluated by electrochemical impedance spectroscopy (EIS), see the Experimental details in the Supporting Information). For comparison, the EIS of pure Celgard and widely reported

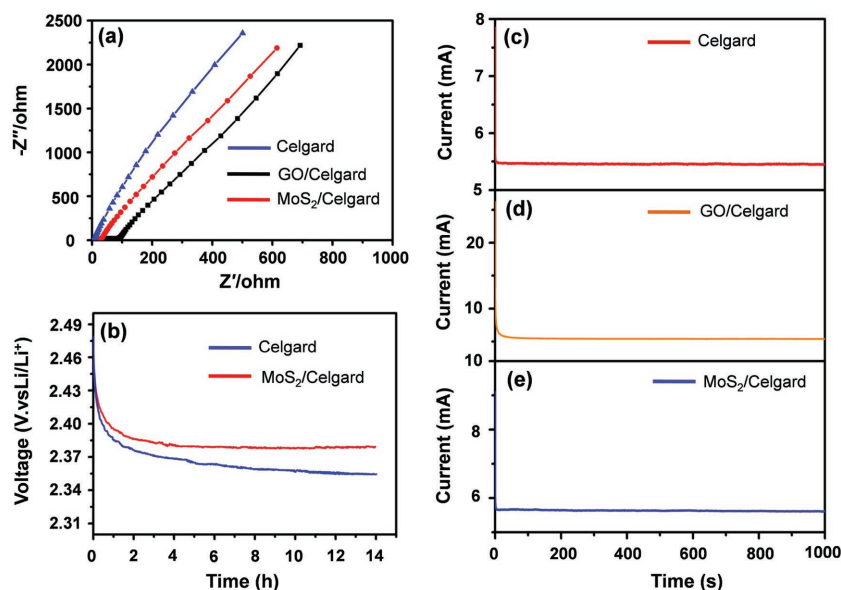


Figure 2. Electrochemical properties of Li-S batteries with different separators. a) Impedance plots estimating lithium conductivity. b) Open circuit voltage profiles showing self-discharge behavior. c) Lithium ions transference number for Celgard, d) GO/Celgard, and e) MoS₂/Celgard separators.

graphene oxide (GO)/Celgard separators were also tested (Figure 2a). The recorded EIS curves for all the three separators exhibit a single semicircle in high frequency region, whereas the MoS₂/Celgard separator shows obviously lower resistance compared with GO/Celgard separator. The quantitative analysis further discloses that the lithium ion conductivity of MoS₂/Celgard separator ($2.0 \times 10^{-1} \text{ mS cm}^{-1}$) is similar to that of pure Celgard separator ($3.3 \times 10^{-1} \text{ mS cm}^{-1}$), which is around one order higher than that of GO/Celgard separator ($3.1 \times 10^{-2} \text{ mS cm}^{-1}$), likely due to the extremely high density of lithium ions on the MoS₂ surfaces caused by lithium ion insertion during exfoliation. Self-discharge phenomenon is also studied by monitoring open circuit voltage (OCV) of the Li-S batteries with Celgard or MoS₂/Celgard separators (Figure 2b). Within a few hours, a drastic decay in the OCV (2.35 V) of the battery with Celgard separator occurs indicative of severe self-discharge. On contrary, the self-discharge phenomenon is efficiently depressed by using MoS₂/Celgard separator with a stable OCV (2.38 V), which is in accordance with the discharge capacity after resting for several hours. It is apparent from Figure S3a (Supporting Information) that batteries with Celgard separator suffer from severe self-discharge and the capacities fall down to 95%, 83%, and 75% after resting for 1, 4, and 14 h, respectively. In contrast, for batteries with MoS₂/Celgard separator, about 99%, 95%, and 91% capacities are respectively retained after keeping the devices rest for 1, 4, and 14 h, clearly showing a good control over the self-discharge phenomenon (Figure S3b, Supporting Information).

Beside the conductivity, the lithium ion transference across the separator is another factor to affect battery performance. To acquire the detailed transference numbers of lithium ions, the Celgard, GO/Celgard, and MoS₂/Celgard separators were sandwiched between two lithium electrodes, and a constant potential of 10 mV was applied. Consequently, a current–time

(*i*–*t*) curve is obtained (Figure 2c–e), in which the transference number is estimated from the ratio of steady state current to initial current. Apparently, the lithium ion transference number of MoS₂/Celgard separator (0.62) is almost similar to that of pure Celgard (0.69) but about three fold higher than GO/Celgard separator (0.21), indicating its excellent lithium ion transport property (Table 1). Next, the lithium ion diffusion coefficients (D_{Li^+}) for Celgard, GO/Celgard, and MoS₂/Celgard separators were quantitatively calculated by a series of cyclic voltammograms (CVs) with different scan rates. As shown in Figure S4 (Supporting Information), the cathodic peaks at 1.8–2.1 V and 2.3–2.4 V are respectively labeled as A and B, while the anodic peak at around 2.4–2.5 V as C. Randles–Sevcik equation^[21] is adopted, and then lithium ion diffusion coefficient is calculated based on the slope of the linear plot of the peak current (I_p) versus the square root of the scan rate ($V^{0.5}$). The value of lithium diffusion coefficients for the batteries with Celgard, GO/Celgard, and MoS₂/Celgard separators are summarized in

Table 1. It is noted from Table 1 that the diffusion coefficient at peak B is almost of the same order of magnitude for GO/Celgard ($2.5 \times 10^{-9} \text{ cm}^2 \text{ s}^{-1}$) and MoS₂/Celgard ($7.6 \times 10^{-9} \text{ cm}^2 \text{ s}^{-1}$) but relatively lower than pure Celgard ($1.2 \times 10^{-8} \text{ cm}^2 \text{ s}^{-1}$). At the peak B of higher voltage that involves formation of PSs, the open pores of pristine Celgard are covered by GO or MoS₂ nanosheets, thus leading to lowered lithium ion diffusion. It is interesting that the diffusion coefficient for MoS₂/Celgard at the peak A of lower voltage ($2.4 \times 10^{-8} \text{ cm}^2 \text{ s}^{-1}$) is higher than both pristine Celgard ($6.5 \times 10^{-9} \text{ cm}^2 \text{ s}^{-1}$) and GO/Celgard ($9.1 \times 10^{-10} \text{ cm}^2 \text{ s}^{-1}$). In fact, at lower voltage the high order PSs convert to solid lithium sulfides. These solid lithium sulfides would easily precipitate at the cathode–separator interface as an insulating layer, thereby hindering lithium ion diffusion.^[23] It is deduced that the MoS₂ nanosheets can provide voids to accommodate various redox species and prevent formation of such insulating layer, resulting in facile lithium ion diffusion. The above observation demonstrates that different with GO

Table 1. Summary of various electrochemical parameters for Celgard, GO/Celgard, and MoS₂/Celgard separators.

Parameters	Celgard	MoS ₂ /Celgard	GO/Celgard
R_o [Ω]	7.38	5.60	7.39
R_{ct} [Ω]	281.90	163.90	220.60
R_{sf} [Ω]	38.28	–	63.05
R'_{sf} [Ω]	118.20	–	–
D_{Li^+} at peak A [$\text{cm}^2 \text{ s}^{-1}$]	6.5×10^{-9}	2.4×10^{-8}	9.1×10^{-10}
D_{Li^+} at peak B [$\text{cm}^2 \text{ s}^{-1}$]	1.2×10^{-8}	7.6×10^{-9}	2.5×10^{-9}
D_{Li^+} at peak C [$\text{cm}^2 \text{ s}^{-1}$]	5.6×10^{-8}	4.9×10^{-8}	2.2×10^{-8}
Li ⁺ conductivity [mS cm^{-1}]	3.3×10^{-1}	2.0×10^{-1}	3.1×10^{-2}
Li ⁺ transfer number	0.69	0.62	0.21

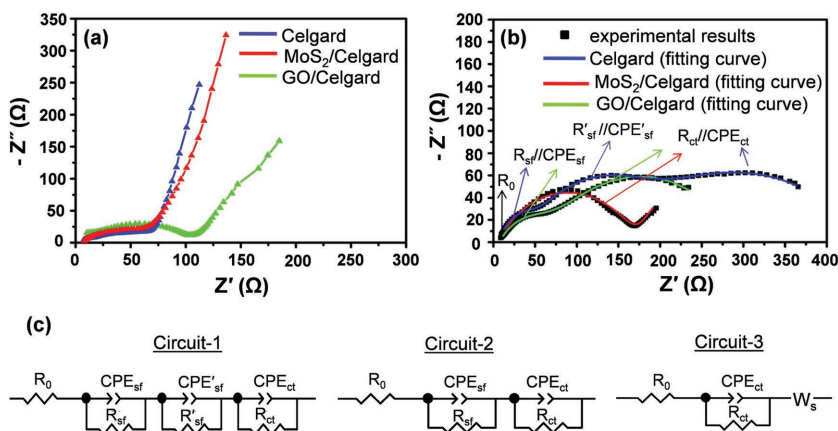


Figure 3. Electrochemical impedance spectra of Li–S batteries a) before and b) after cycling using Celgard, GO/Celgard, and MoS₂/Celgard separators, and c) corresponding equivalent circuits after cycling. Equivalent circuit-1 stands for Celgard, circuit-2 represents GO/Celgard, and circuit-3 refers to MoS₂/Celgard.

sheets, introduction of MoS₂ does not notably degrade lithium ion diffusion, which is reasonable considering its high lithium conductivity and good resistance to lithium sulfides formation (Figure 1a).

The effect of MoS₂ layer on the battery's electrochemical kinetics before and after cycling is also explored by EIS measurement (Figure 3a,b). The EIS spectra for the batteries with Celgard, GO/Celgard or MoS₂/Celgard separators after cycling are modeled with equivalent circuits (Figure 3c), and the results are summarized in Table 1. In these equivalent circuits, R_0 is interphase-contact resistance of the electrolyte and battery, R_{ct} is the charge transfer resistance, R_{sf} and R'_{sf} are the surface film resistances, W_s is the Warburg impedance, while CPE represents the corresponding constant phase element about the double layer capacitance.^[35,36]

It is clearly seen from Figure 3a that before cycling, batteries using Celgard and MoS₂/Celgard separators have a considerably lower bulk resistivity ($\approx 60\text{--}65\ \Omega$) compared to GO/Celgard ($\approx 95\ \Omega$), suggesting fast lithium ion diffusion. However, after cycling the battery with Celgard separator shows three semicircles (Figure 3b). The semicircle in high frequency (R_{sf}/CPE_{sf}) is related to formation of an insulating layer of solid Li₂S₂/Li₂S between separator and cathode, while the semicircle in middle frequency (R'_{sf}/CPE'_{sf}) is attributed to formation of another insulating layer on lithium anode surface due to diffusion of PSs, and the third semicircle in low frequency (R_{ct}/CPE_{ct}) is assigned to the charge transfer resistance (circuit-1 in Figure 3c). After introduction of GO layer, the PSs migration is partially suppressed, indicated by existence of only two semicircles (green curve in Figure 3b); however, the R_{sf} value considerably increases (Table 1) because of solid Li₂S₂/Li₂S formation. This result is in good agreement with analysis

on the lithium ion diffusion coefficients (Figure S4, Supporting Information). Note-worthily, the battery using MoS₂/Celgard separator possesses only one semicircle in high frequency region (red curve in Figure 3b), and the resultant lower R_{ct} value manifests facile reaction kinetics.

Armed with the above results, we are confident that MoS₂/Celgard separator would be an ideal ion sieve, which selectively allows lithium ions passing through while efficiently suppressing undesired PSs migration. Hence, the electrochemical property of the Li–S batteries with MoS₂/Celgard separator was studied with standard CR2032 coin cells using sulfur-carbon black cathode with 65% sulfur loading (Figure 4). As shown by the typical CV curve at a scan rate of $0.2\ \text{mV s}^{-1}$ (Figure 4a), the reduction scan is composed of two well-defined peaks at 2.3 and

2.0 V, representing reduction of elemental sulfur to soluble high order PSs (Li₂S_{*n*}, $4 < n < 8$) and their further reduction to solid lithium sulfides (Li₂S₂/Li₂S), respectively.^[3,18] In the subsequent anodic scan, one oxidation peak at 2.5 V is discerned, corresponding to conversion of PSs to elemental sulfur with facile electrochemical kinetics. The galvanostatic charge/discharge study of the Li–S battery with MoS₂/Celgard separator is then performed at a constant current rate of 0.2 C (Figure 4b). Consistent with the CV curve, the discharge/charge curves consist of two reduction plateaus and one long oxidation plateau, representing the redox reactions of a typical Li–S battery. The cyclic performance of the Li–S battery with Celgard, GO/Celgard or MoS₂/Celgard separators is further evaluated at a high

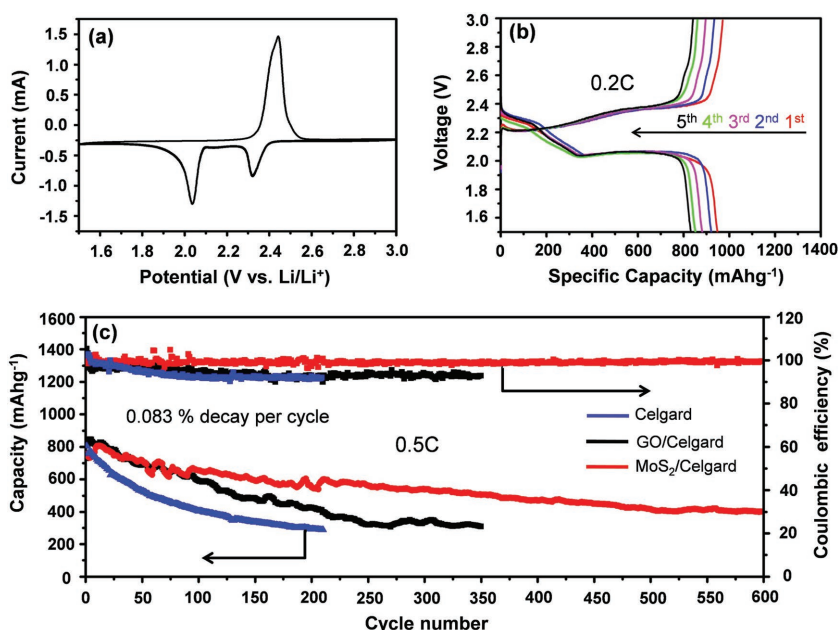


Figure 4. a) Cyclic voltammogram profile for Li–S battery with MoS₂/Celgard separator at scan rate of $0.2\ \text{mV s}^{-1}$. b) Galvanostatic charge–discharge profiles at a rate of $0.2\ \text{C}$. c) Long life cycle test for Celgard, GO/Celgard, and MoS₂/Celgard separators at $0.5\ \text{C}$.

current rate of 0.5 C. As displayed in Figure 4c, the battery with Celgard separator delivers an initial discharge capacity of 804 mAh g⁻¹, and drastically falls to 290 mAh g⁻¹ after 208 cycles with a poor Coulombic efficiency of as low as 91%, indicative of high order PSs shuttle.^[28] After the introduction of GO layer a slight improvement occurs and the Coulombic efficiency (93%) remains higher than pure Celgard. However, the initial capacity drastically falls from 846 to 308 mAh g⁻¹ over 350 cycles. In contrast, the battery with MoS₂/Celgard separator delivers an initial discharge capacity of 808 mAh g⁻¹ (after activation in the first few cycles), which is maintained to be 401 mAh g⁻¹ after 600 cycles with an average capacity fading of only 0.083% per cycle. Additionally, the extraordinarily high Coulombic efficiency (>99.5%) for the battery with MoS₂/Celgard separator during the whole 600 cycles demonstrates efficient blocking of soluble PSs.^[37] Significantly, the electrochemical performance of the battery is easily optimized by altering membrane thickness. The membranes with different thickness could be fabricated by filtering different amount of MoS₂ solution (Figure S5, Supporting Information). It is seen from Figure S6 (Supporting Information) that a gradual increase in the thickness of the MoS₂ membrane gives rise to enhanced stability as well as the Coulombic efficiency. However, when the thickness is increased to 500 nm, the initial capacity obviously decreases, which is caused by an increase in the diffusion path length and internal resistance (Figure S6, Supporting Information).^[1,21,38] Finally, the rate performance of the battery with MoS₂/Celgard is investigated at different current densities. As displayed in Figure S7 (Supporting Information), the battery delivers discharge capacities of 1471, 1039, 770 and 550 mAh g⁻¹ at 0.1, 0.2, 0.5, and 1 C, respectively. Moreover, a discharge capacity of 931 mAh g⁻¹ could be recovered when the rate is abruptly turned back to 0.1 C, indicating good rate capability. Evidently, the high Coulombic efficiency and long cycle stability of Li-S battery with MoS₂/Celgard separator should be attributed to its high lithium ion conductivity, fast lithium transference across the separator, and facile lithium diffusion.

To explore the interaction between PSs and MoS₂, the MoS₂/Celgard separator from a discharged battery is used for XPS characterization. As shown in Figure S8 (Supporting Information), the Mo 3d XPS spectra of the MoS₂/Celgard separator are composed of Mo 3d_{5/2} (228.7 eV) and Mo 3d_{3/2} (232.3 eV) (Figure S8a, Supporting Information). After discharging, the Mo 3d peaks show a slight shifting to negative binding energy (Mo 3d_{5/2} to 228.5 eV and Mo 3d_{3/2} to 232.0 eV), suggesting the Mo-S_n²⁻ interaction (Figure S8b, Supporting Information).^[35,39] The XPS result reveals that the stacked structure of the MoS₂ membrane not only acts as ion sieve to block PSs but also provides free spaces to accommodate various PSs intermediates via physiochemical interaction, thus preventing their diffusion into the electrolyte, depressing the shuttle effect and enhancing the performance of the battery.^[38,40]

In conclusion, a MoS₂/Celgard composite separator has been constructed by simply filtering exfoliated MoS₂ solution through Celgard substrate. Thanks to the high density of lithium ions on MoS₂ surface, this composite separator exhibits high lithium conductivity, fast lithium diffusion, and facile transference across the separator. When used in Li-S batteries, the separator is proved to be highly efficient for depressing PSs

shuttle, leading to high Coulombic efficiency and long cycle stability. As seen from the comparison (Table S1, Supporting Information), with 65% of sulfur loading, our battery with MoS₂/Celgard separator delivers an initial capacity of 808 mAh g⁻¹ and a substantial capacity of 401 mAh g⁻¹ after 600 cycles, corresponding to only 0.083% of capacity decay per cycle that is comparable to the best reported results so far. In addition, the Coulombic efficiency remains more than 99.5% during all 600 cycles, disclosing an efficient ionic sieve preventing PSs migration to the anode while having negligible influence on lithium ions transference across the separator. The strategy demonstrated in this work will open the door toward developing efficient separators with flexible 2D materials beyond graphene for energy-storage devices.

Supporting Information

Supporting Information is available from the Wiley Online Library or from the author.

Acknowledgements

Z.A.G. and X.H. contributed equally to this work. This work was supported by the National Natural Science Foundation of China (Grant No. 51472054, L.L.), National Key Basic Research Program of China (Grant Nos. 2014CB931801 and 2016YFA0200700, Z.Y.T.), National Natural Science Foundation of China (Grant Nos. 21475029 and 91427302, Z.Y.T.), Frontier Science Key Project of the Chinese Academy of Sciences (Grant No. QYZDJ-SSW-SLH038, Z.Y.T.), Instrument Developing Project of the Chinese Academy of Sciences (Grant No. YZZ201311, Z.Y.T.), CAS-CSIRO Cooperative Research Program (Grant No. GJHZ1503, Z.Y.T.), and the "Strategic Priority Research Program" of Chinese Academy of Sciences (Grant No. XDA09040100, Z.Y.T.).

Received: December 17, 2016

Revised: February 12, 2017

Published online:

- [1] L. Qie, A. Manthiram, *Adv. Mater.* **2015**, *27*, 1694.
- [2] X. Liang, C. Hart, Q. Pang, A. Garsuch, T. Weiss, L. F. Nazar, *Nat. Commun.* **2015**, *6*, 5682.
- [3] X. Gao, J. Li, D. Guan, C. Yuan, *ACS Appl. Mater. Interfaces* **2014**, *64*, 154.
- [4] J. Guo, Z. Yang, Y. Yu, H. D. Abuña, L. A. Archer, *J. Am. Chem. Soc.* **2013**, *135*, 763.
- [5] Z. Li, J. Zhang, X. W. Lou, *Angew. Chem., Int. Ed.* **2015**, *54*, 12886.
- [6] X. Ji, K. T. Lee, L. F. Nazar, *Nat. Mater.* **2009**, *8*, 500.
- [7] C.-P. Yang, Y.-X. Yin, H. Ye, K.-C. Jiang, J. Zhang, Y.-G. Guo, *ACS Appl. Mater. Interfaces* **2014**, *6*, 8789.
- [8] S. Xin, L. Gu, N.-H. Zhao, Y.-X. Yin, L.-J. Zhou, Y.-G. Guo, L.-J. Wan, *J. Am. Chem. Soc.* **2012**, *134*, 18510.
- [9] L. Sun, M. Li, Y. Jiang, W. Kong, K. Jiang, J. Wang, S. Fan, *Nano Lett.* **2014**, *14*, 4044.
- [10] G. He, B. Mandlmeier, J. Schuster, L. F. Nazar, T. Bein, *Chem. Mater.* **2014**, *26*, 3879.
- [11] C. Zhang, H. B. Wu, C. Yuan, Z. Guo, X. W. Lou, *Angew. Chem., Int. Ed.* **2012**, *51*, 9592.
- [12] L. Qie, A. Manthiram, *Adv. Mater.* **2015**, *27*, 1694.
- [13] G. Qu, J. Cheng, X. Li, L. Huang, W. Ni, Z. Wang, B. Wang, *ACS Appl. Mater. Interfaces* **2015**, *7*, 16668.

- [14] Y. Fu, A. Manthiram, *J. Phys. Chem. C* **2012**, *11*, 68910.
- [15] W. Zhou, Y. Yu, H. Chen, F. J. DiSalvo, H. D. Abruña, *J. Am. Chem. Soc.* **2013**, *135*, 16736.
- [16] Y. Yang, G. Yu, J. J. Cha, H. Wu, M. Vosgueritchian, Y. Yao, Z. Bao, Y. Cui, *ACS Nano* **2011**, *5*, 9187.
- [17] J. Zhou, R. Li, X. Fan, Y. Chen, R. Han, W. Li, J. Zheng, B. Wang, X. Li, *Energy Environ. Sci.* **2014**, *7*, 2715.
- [18] Z. A. Ghazi, L. Zhu, H. Wang, A. Naeem, A. M. Khatkhat, B. Liang, N. A. Khan, Z. Wei, L. Li, Z. Tang, *Adv. Energy Mater.* **2016**, 1601250.
- [19] H. Liao, H. Ding, B. Li, X. Ai, C. Wang, *J. Mater. Chem. A* **2014**, *2*, 8854.
- [20] G. Zhou, L. Li, D.-W. Wang, X.-Y. Shan, S. Pei, F. Li, H.-M. Cheng, *Adv. Mater.* **2015**, *27*, 641.
- [21] J.-Q. Huang, T.-Z. Zhuang, Q. Zhang, H.-J. Peng, C.-M. Chen, F. Wei, *ACS Nano* **2015**, *9*, 3002.
- [22] Z. Yunbo, M. Lixiao, N. Jing, X. Zhichang, H. Long, W. Bin, Z. Linjie, *2D Mater.* **2015**, *2*, 024013.
- [23] G. Zhou, S. Pei, L. Li, D.-W. Wang, S. Wang, K. Huang, L.-C. Yin, F. Li, H.-M. Cheng, *Adv. Mater.* **2014**, *26*, 625.
- [24] G. Zhou, L. Li, C. Ma, S. Wang, Y. Shi, N. Koratkar, W. Ren, F. Li, H.-M. Cheng, *Nano Energy* **2015**, *11*, 356.
- [25] P. G. Bruce, S. A. Freunberger, L. J. Hardwick, J.-M. Tarascon, *Nat. Mater.* **2012**, *11*, 19.
- [26] K. Zhang, Q. Li, L. Zhang, J. Fang, J. Li, F. Qin, Z. Zhang, Y. Lai, *Mater. Lett.* **2014**, *121*, 198.
- [27] W. Li, J. Hicks-Garner, J. Wang, J. Liu, A. F. Gross, E. Sherman, J. Graetz, J. J. Vajo, P. Liu, *Chem. Mater.* **2014**, *26*, 3403.
- [28] J. Yoo, S.-J. Cho, G. Y. Jung, S. H. Kim, K.-H. Choi, J.-H. Kim, C. K. Lee, S. K. Kwak, S.-Y. Lee, *Nano Lett.* **2016**, *16*, 3292.
- [29] S. Bai, X. Liu, K. Zhu, S. Wu, H. Zhou, *Nat. Energy* **2016**, *1*, 16094.
- [30] H. Li, Z. Yin, Q. He, H. Li, X. Huang, G. Lu, D. W. H. Fam, A. I. Y. Tok, Q. Zhang, H. Zhang, *Small* **2012**, *8*, 63.
- [31] J. Feng, X. Qian, C.-W. Huang, J. Li, *Nat. Photonics* **2012**, *6*, 866.
- [32] T. Stephenson, Z. Li, B. Olsen, D. Mitlin, *Energy Environ. Sci.* **2014**, *7*, 209.
- [33] H. Tang, J. Wang, H. Yin, H. Zhao, D. Wang, Z. Tang, *Adv. Mater.* **2015**, *27*, 1117.
- [34] G. Eda, H. Yamaguchi, D. Voiry, T. Fujita, M. Chen, M. Chhowalla, *Nano Lett.* **2011**, *11*, 5111.
- [35] J. Sun, Y. Sun, M. Pasta, G. Zhou, Y. Li, W. Liu, F. Xiong, Y. Cui, *Adv. Mater.* **2016**, *28*, 9797.
- [36] M. Kazazi, M. R. Vaezi, A. Kazemzadeh, *Ionics* **2014**, *20*, 635.
- [37] Q. Pang, L. F. Nazar, *ACS Nano* **2016**, *10*, 4111.
- [38] H. Al Salem, G. Babu, C. V. Rao, L. M. R. Arava, *J. Am. Chem. Soc.* **2015**, *137*, 11542.
- [39] A. Vizintin, M. Lozinšek, R. K. Chellappan, D. Foix, A. Krajnc, G. Mali, G. Drazic, B. Genorio, R. Dedryvère, R. Dominko, *Chem. Mater.* **2015**, *27*, 7070.
- [40] J. Song, M. L. Gordin, T. Xu, S. Chen, Z. Yu, H. Sohn, J. Lu, Y. Ren, Y. Duan, D. Wang, *Angew. Chem., Int. Ed.* **2015**, *54*, 4325.